# CHAPTER 7

# Case Study
## (DESIGN AND SIMULATION, TECHNOLOGY, CHARACTERIZATION)

by: Hans-Joachim Wagner
Institute for Micro- and Information Technology (IMIT),
VS-Villingen, Germany

## 7.1 Introduction

A resonant force sensor with semidigital frequency output based on a triple-beam resonator structure in silicon with piezoelectric ZnO thin film **[7.20]** is presented as example for this case study.
Resonant sensors in quartz and silicon exhibit a wide field of applications and special benefits like large gauge factors, high resolution and a semidigital frequency output **[7.1, 7.2]**. The resonant force sensor described here is based on the principle of a resonator being excited in a specific flexural vibration mode. It changes its resonance frequency when mechanical stress is applied. One key aspect in the design of resonant sensor devices is a high mechanical quality factor, leading to high resolution and sensitivity. This can be achieved by placing the resonator in an evacuated cavity **[7.3]** and/or by using a special resonator design **[7.4]**. Disadvantages of vacuum-encapsulated resonator designs are the quite complicated fabrication technology and additionally arising packaging problems.

### Cooperation with industrial partners

This case study is based on a project, supported by the Bundesministerium für Forschung und Technologie (BMFT), Germany, running at the IMIT from from mid 1989 to 1992. In cooperation with four industrial partners (Bizerba-Werke Wilhelm Kraut GmbH & Co., Balingen; Robert Bosch GmbH, Stuttgart; MotoMeter GmbH, Leonberg; Gesellschaft für Mikrotechnik und Sensorik mbH, St. Georgen), the aims of development were fixed. The main topic of this project was the installation of the technology to produce prototypes of resonant sensors with frequency output and investigations for their application as, i.e. force sensitive devices for weighing-units.

**Specifications of the force sensor device**

Initially the following features for a micromachined force sensor in quartz or silicon were claimed (see **Table 1**):

**Table 7.1** Features of the force sensor device (-10 °C to +40 °C).

| | |
|---|---|
| Force load | 0-5, 10, 20, 30, 40 [N] |
| Overload protection | 5 x |
| Linearity error | < 50 ppm |
| Hysteresis error | < 50 ppm |
| Creeping error | < 50 ppm |
| Temperature coeff. offset | < 12 ppm / °C |
| Temperature coeff. (TKC) | < 5 ppm / °C |
| Measuring time | < 100 ms |
| Balance resolution | 100.000 digits |

**Consideration of the alternative materials silicon and quartz**

Some major differences between quartz and silicon as resonator material are the following (see also [7.21]):

Quartz, in contrast to silicon, is itself a piezoelectric material. This property can be used for excitation and detection of the vibration: only conducting electrodes have to be deposited on the quartz structure in order to obtain a usable resonator. Silicon resonators need special excitation and detection elements (electromechanical transducers), for which many alternatives can be found.

Further, quartz can be cut in a special way to minimize temperature effects. In this way, resonators having a temperature coefficient of 25 ppm over the temperature range from - 55 °C to 105 °C can be realized without any compensation. Silicon, on the other hand, has a temperature dependent Youngs's modulus of -94 ppm/ °C. In many cases, this results in a temperature coefficient of the resonance frequency of -47 ppm/ °C. Moreover, the transducer elements, which consist of "strange" materials will generally have different temperature coefficients, making things only worse, or at least hard to control.

It is often advanced that, in the case of silicon, electronics for power supply, data processing and feed back can be realized on the same chip as the sensor, which has advantages with respect to the signal to noise ratio. At the same time however, much of the technological flexibility has to be sacrificed in favour of the compatibility with an IC process.

Bulk force sensor devices fabricated in monocrystalline quartz normally use a double-ended tuning-fork (DETF) design (see **Fig. 1**) in order to balance the in-plane motions of the tuning-fork tines and to cancel out moments that are responsible for energy dissipation into the resonator mount [7.5].

Since quartz is piezoelectric, there is an easy way to excite and detect the vibration of the resonator and to operate the quartz force sensor as an electrical one-port in a feedback loop of an oscillator circuit.

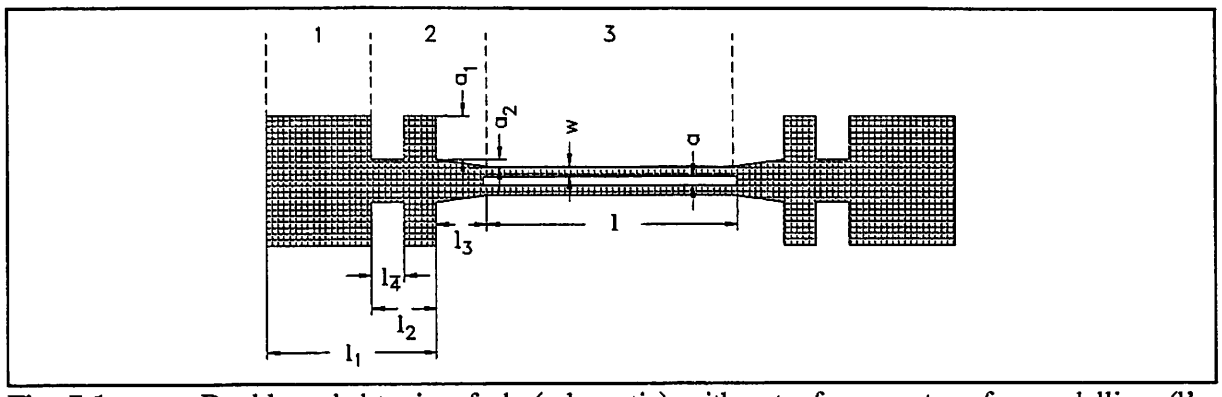


**Fig. 7.1** Double-ended-tuning fork (schematic) with set of parameters for modelling (l's, lengths of the resonator; w, width; a's, distances; 1, clamping region; 2, decoupling zone; 3, resonator).

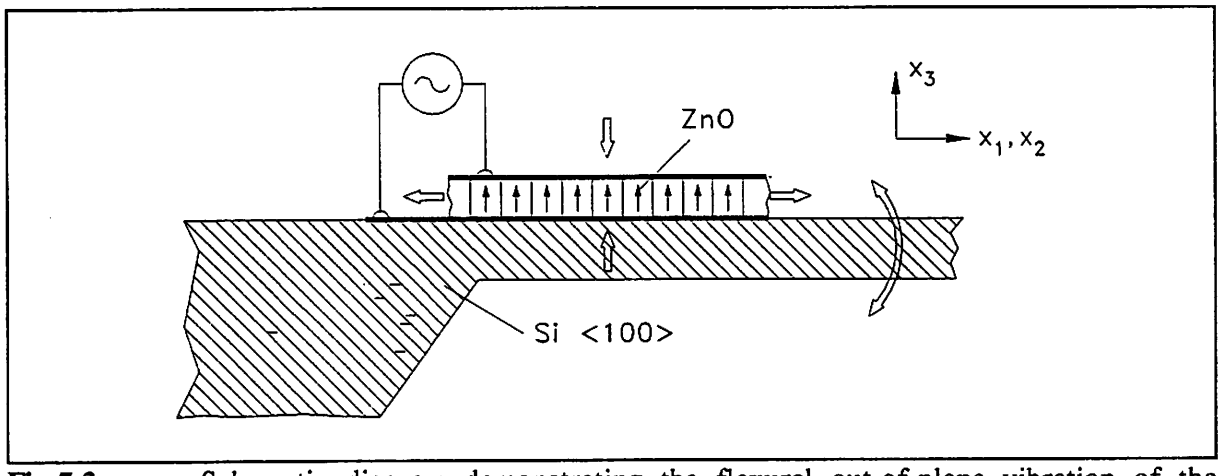


**Fig 7.2** Schematic diagram demonstrating the flexural out-of-plane vibration of the silicon/ZnO bimorph excited due to the piezoelectric transversal ($d_{31}$) effect.

The fact that silicon is a non-piezoelectric material leads to the necessity to deposit additional piezoelectric thin-film layers onto the beams to excite them. In this work we used r.f. sputtered zinc oxide (ZnO) thin films. Due to the induced bending moments of the silicon/ZnO bimorph, the flexural vibrations are out-of-plane (see **Fig. 2**). To achieve a cancellation of moments and shear forces at the clamped ends, in this case more than two beams are obviously necessary. A resonator comprising a triple or a quadruple beam structure is well suited for this purpose **[7.6 - 7.8]**. We report on the first realisation of piezoelectrically driven resonant silicon force sensors with triple-beam design **[7.20]**, where the centre beam has twice the width of the two outer beams and vibrates in antiphase with them.

**Choice of excitation principle**

The variety of excitation and detection principles is discussed in **Chapter 5.**

In the above mentioned project we promoted the electrothermal and the piezoelectric excitation principle. Here we describe the piezoelectric excitation/detection principle. Some materials like AlN, ZnO, PZT are well suited for this purpose.

Due to interesting material properties, wide-spread applications, and many references concerning ZnO, the piezoelectric excitation of the resonator operating in an antisymmetric

vibration mode is realized by thin-film zinc oxide layers.

## 7.2 Design of the piezoelectrically driven triple beam resonator

An advantage of the triple-beam design is a high mechanical quality factor combined with high force sensitivity due to the antisymmetric vibration mode and the load-dependent stress concentration in the triple beam.
The schematic diagram of the triple-beam sensor device is illustrated in **Fig. 7.3**. Moreover, the sensor includes two strengtening shunts with bulk thickness for overload protection and a laser-cut mounting hole at each side of the bulk area, allowing uniaxial force loading.
The triple-beam resonator is connected to the bulk material on both sides via flexible decoupling zones. The thickness of the decoupling zone is equal to that of the beams, allowing energy transfer during vibration. The length of the decoupling zones was optimized by finite-element (FE) modelling.

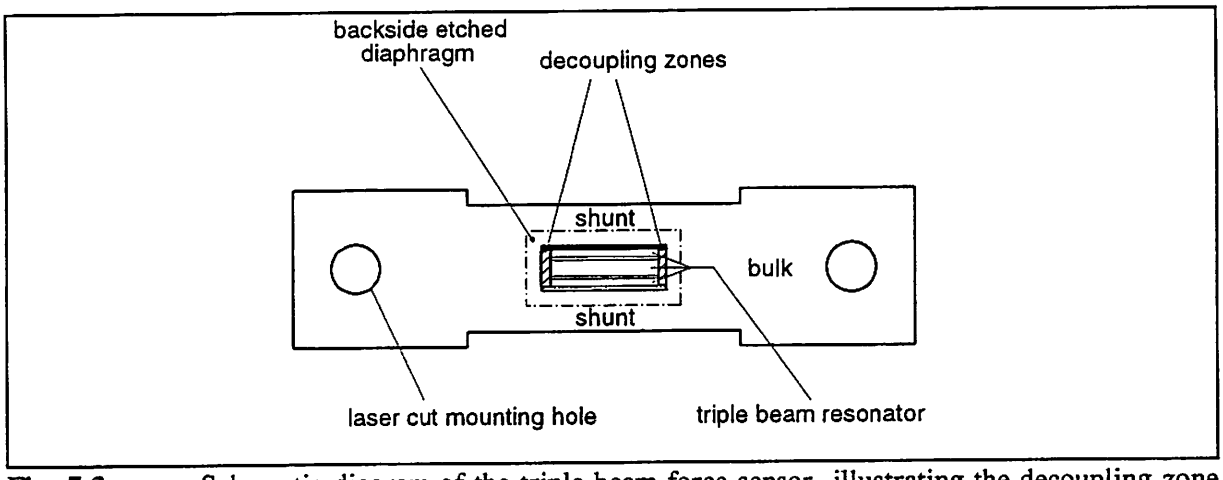


**Fig. 7.3** Schematic diagram of the triple-beam force sensor, illustrating the decoupling zone from the bulk area with laser-cut mounting holes.

## 7.3 Modeling of the triple beam resonator with finite element analysis methods

Extensive finite-element modelling has been carried out to determine the static and dynamic behaviour and to obtain optimum sensor performance.
A numerical method such as finite-element analysis can be used to predict the sensor characteristics with reasonable accuracy and to analyze geometric modifications on the sensor performance. The general-purpose finite-element software program ANSYS **[7.9]** was used to predict the modal behaviour of the triple-beam resonator. The eigenfrequencies and the associated complex vibration mode shapes were determined in modal analyses. In combination with static analyses the force sensitivities were calculated and compared to a single-beam force sensor with the same resonator dimensions. In particular, the influence of the clamping region on mechanical decoupling of the resonator from the supporting bulk material was analyzed.
Mechanical decoupling of a single-beam resonator was proposed by *Albert* **[7.10]**. To minimize energy dissipation coupled into the supporting structure, a mechanical isolation system was employed in the sensor design. Multiple-beam resonators like DETF, triple- or quadruple-beam types include inherent dynamic moment cancellation when they are excited

in an antisymmetric vibration mode. A major task of the numerical modelling was to design an appropriate mechanical decoupling zone for the triple-beam resonator. At the same time, a mode spectrum of the whole sensor device preventing mode interferences caused by a force-dependent shift in resonance frequency had to be found [7.11].
The dependence of the resonance frequencies for the first three flexure modes on decoupling zone length is shown in **Fig. 7.4**. The fundamental flexure mode of the beams vibrating symmetrically in phase is denoted M1. A spurious overtone mode M2 occurs between mode M1 and the antisymmetric sensor mode M3. Using an FE model with 2-D plastic shell elements and assuming isotropic material behaviour, the resonance frequencies and flexure mode shapes were calculated.

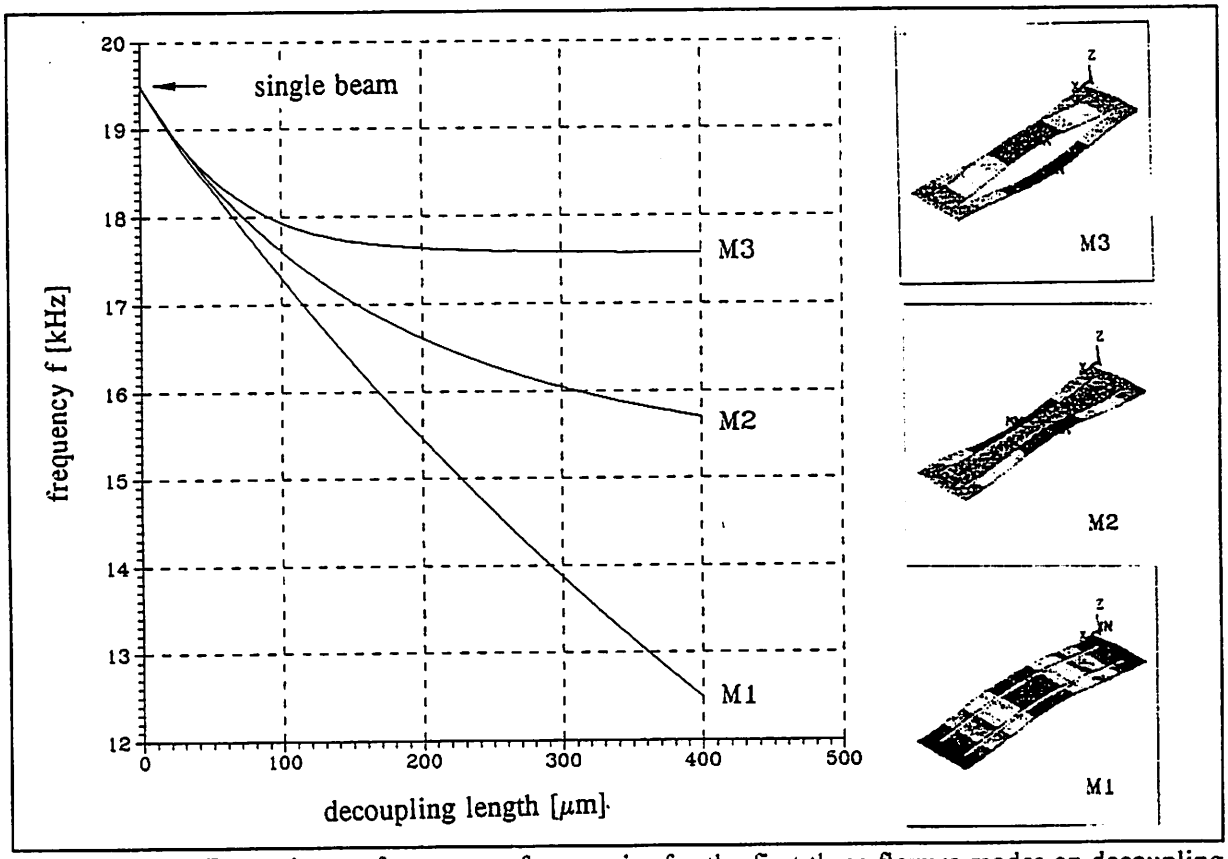


**Fig. 7.4** Dependence of resonance frequencies for the first three flexure modes on decoupling length (M1, fundamental mode; M2, spurious overtone mode, M3, antisymmetric sensor mode).

The analysed triple-beam resonator has a length of 3 mm, a thickness of 20 $\mu$m and beam widths of 400 and 200 $\mu$m, respectively. The distance between the beams is 50 $\mu$m. The length of the decoupling zone is 200 $\mu$m (i.e., 6.7% of beam length), causing mechanical decoupling and leading to a sufficient splitting of the vibration modes. This yields an increased unimodal behaviour of the resonant sensor. The resonance frequency of the single-beam resonator is reached for vanishing decoupling length.
The numerically calculated results for single-beam and triple-beam resonant force sensors are summarized in **Table 7.2**, comparing the static and dynamic behaviour of both resonator types. The fundamental flexure resonance frequencies and their shift due to mechanical loading (force: 1 N) were calculated. In comparison to the single-beam force sensor, the triple-beam configuration exhibits a larger force sensitivity due to stress concentration, mentioned by Kirman [7.6]. The stress within the single beam is about 56 MPa and increases to about 63 MPa due to the smaller cross section of the triple-beam resonator.

In contrast to single-beams, the triple-beam exhibits increased force sensitivities with higher vibration mode numbers. Furthermore, the force sensitivity of the sensor device is adjustable by adequate selection of the resonator thickness in combination with the widths of the two suspending shunts for overload protection.

**Table 7.2** Comparison of the numerically calculated static and dynamic characteristics for single-beam and triple- beam force sensors (decoupling length, 200 $\mu$m).

| Characteristic | Single-beam resonator | Triple beam resonator | | |
|---|---|---|---|---|
| Mode | fundamental | M1 | M2 | M3 |
| Frequency [kHz] | 19.48 | 15.51 | 16.62 | 17.61 |
| Sensitivity [kHz/N] | 14.95 | 15.43 | 15.55 | 15.85 |
| Elongation [$\mu$m] | 0.98 | 1.27 | | |
| Stress for F=1N [MPa] | 56 | 63 | | |

## 7.4 Thin-film ZnO as piezoelectric transducer

Piezoelectric thin-film ZnO is a promising and widely used material for electromechanical transducers for high-frequency surface acoustic wave (SAW) as well as for low-frequency bulk acoustic wave (BAW) applications **[7.12, 7.13]**. In this work the transverse piezoelectric effect of highly oriented polycristalline ZnO layers is utilized for exciting the flexural vibration modes (M1, M2, M3) of the triple-beam resonator. Schematic cross-sectional views demonstrating the thin-film multilayer structure and the contacts to the electrodes of the triple-beam force sensor devices are shown in **Fig. 7.5**.

**Development of a zincoxide sputter deposition process**

In order to achieve an optimum electromechanical coupling, the ZnO, crystallizing in hexagonal wurtzite lattice structure, has to be grown with the *c*-axis perpendicular to the film plane and the silicon substrate, respectively. For deposition of well-oriented 3 $\mu$m thick ZnO films, we used a planar r.f. magnetron sputtering system. In **Fig. 7.6** Bragg reflection analysis measurements of thin sputtered films are shown, revealing a high *c*-axis orientation of the ZnO. From a Gaussian fit on the peaks enveloping the curve, an orientation distribution with a FWHM of 0.28° was calculated. A pure (99,999%) ZnO target and a mass-spectrometer-monitored $Ar/O_2$ sputter gas mixture was used.

**Development of a zincoxide wet etching process**

The etching and patterning of the ZnO layer are performed in a stirred solution of HAc, $H_3PO_4$ and $H_2O$ **[7.15]**. The lateral underetching (several microns) of the photoresist mask had to be considered in the mask layout.

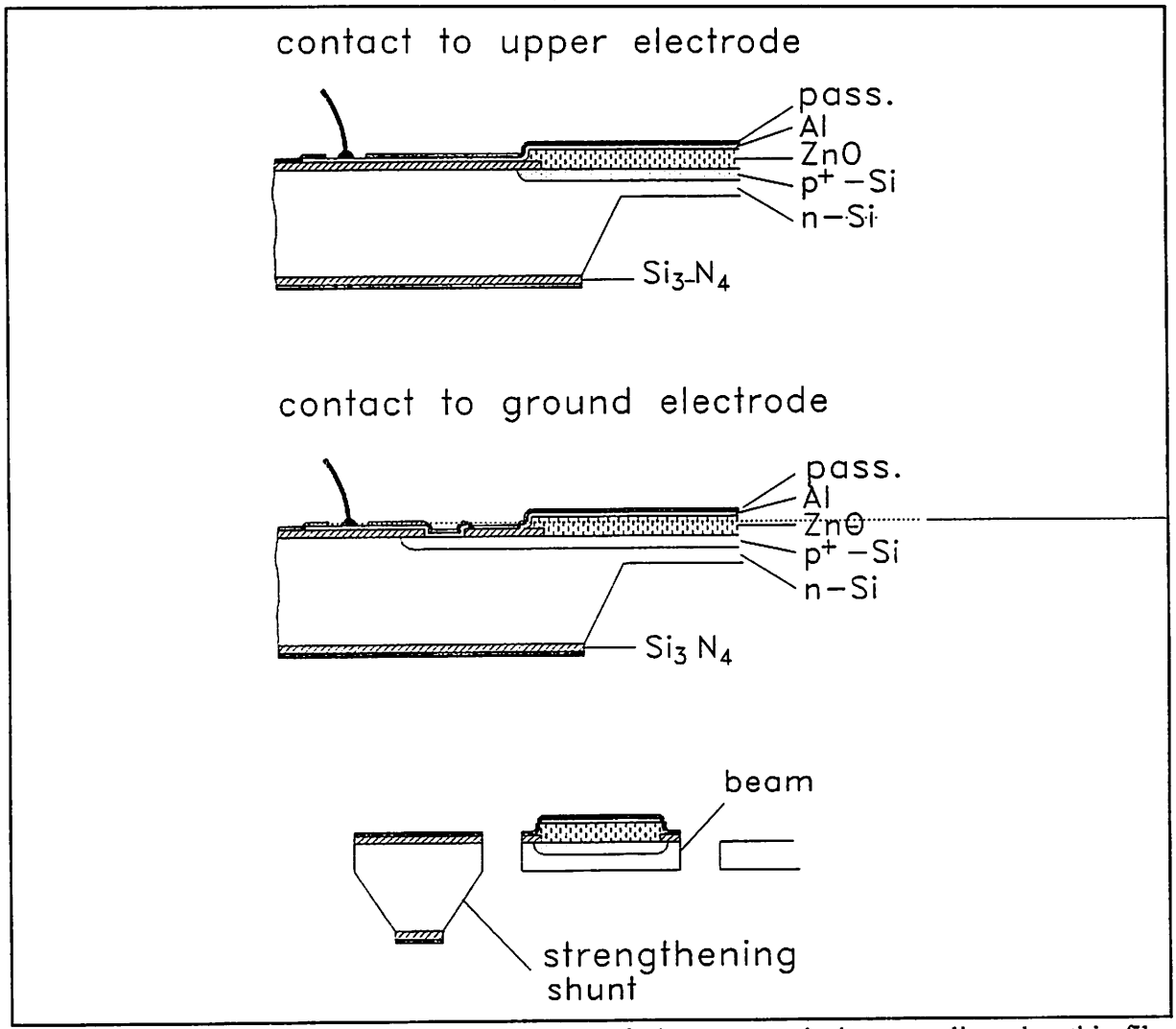


**Fig. 7.5** Schematic cross-sectional views of the sensor device revealing the thin-film multilayers for realization of triple-beam sensors with zinc oxide excitation.

## 7.5 Fabrication sequence

The fabrication process of these triple-beam resonators can be devided into a front-side and a reverse-side process, comparable to that described by *van Mullem et al.* **[7.14]**. Starting with double-faced polished n-type <100> silicon wafers (4 in), the patterning and $p^{++}$-doping of the ground electrode areas separated form each other on both sides of the triple-beam are carried out on the front side of the silicon substrates.
A sputtered and patterned Al metallization layer followed by $SiO_2/S_3N_4$ passivation layers is used as the top electrode contact for the ZnO transducer film.
After completing the planar front-side process, anisotropic wet KOH etching from the reverse side is applied to produce the desired beam thickness of approximately 20 $\mu$m. During this etching process the front side of the substrate is protected by an O-ring sealed wafer protection box comparable to the apparatus described by *Kung et al.* **[7.16]**. In the following process step the triple-beam resonator structure is separated by plasma-etching the diaphragm from the front side. In order to perform the investigations concerning the influence of the clamping region on the dynamic sensor behaviour, a possibility for flexible redesign had to be considered. This could be achieved by changing only the photolithographic mask defining the plasma etched areas.

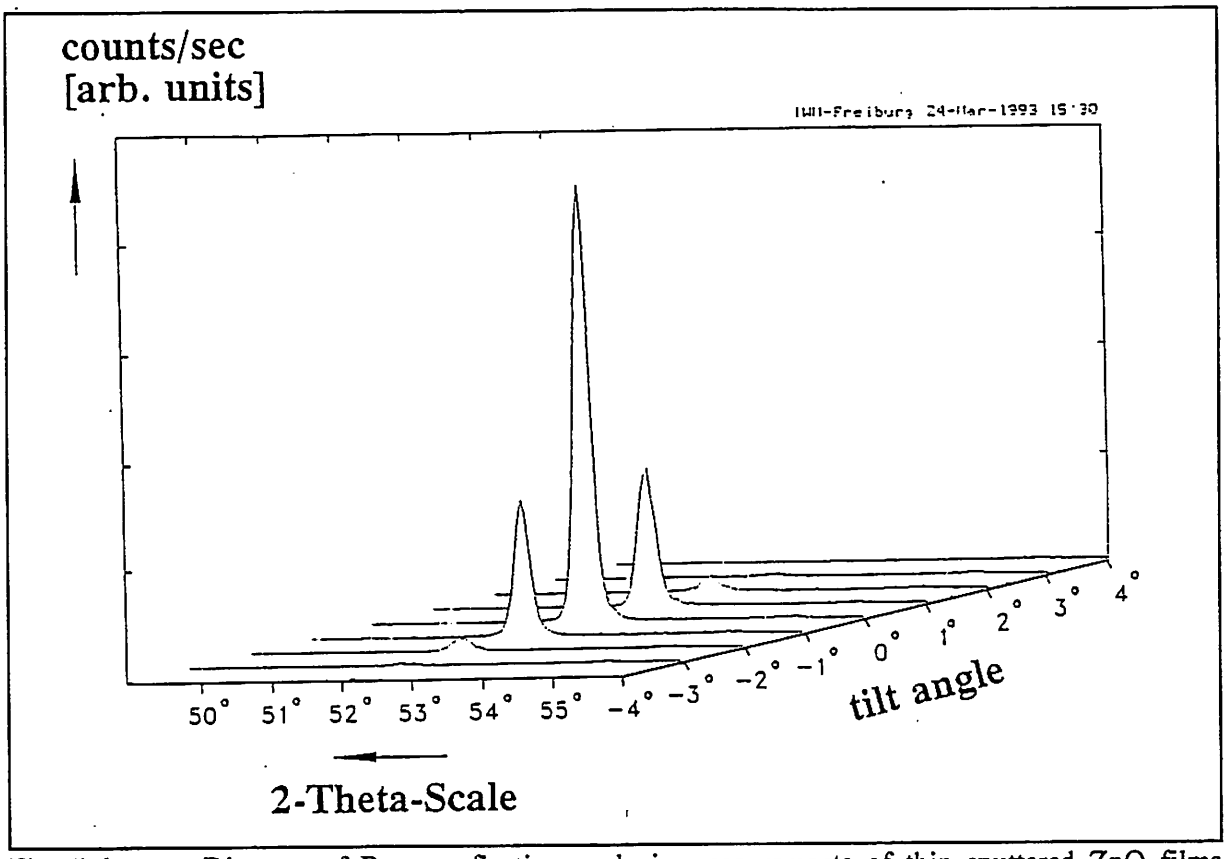


**Fig. 7.6** Diagram of Bragg reflection analysis measurements of thin sputtered ZnO films revealing a high c-axis orientation.

## 7.6 Mounting to a force measurement unit

A micrograph of the sensor device revealing the electrode patterns and bonding pads is shown in **Fig. 7.7.**
A specially developed laser-cutting process is applied to release the sensor devices and to realize mounting holes in the sensor bulk material (see also **Fig. 7.3**). These precisely cut mounting holes provide force measurements with uniaxial application of an external load. The sensor mounting, schematically shown in **Fig. 7.8**, is suitable for hysteresis-free force measurements.

## 7.7 Experimental results

Several resonator designs have been fabricated to study mechanical decoupling from the clamping region.

**Optical and electrical measurement techniques**
Several measurement techniques were utilized for the mechanical and electrical characterization of the ZnO thin films. The mechanical properties of ZnO were estimated with indenter measurements, resulting in reduced Young's modulus $E/(1-\nu^2)$ of 125-173 GPa for 2-3 $\mu$m thin layers. Assuming a mean value of $\nu = 0.36$ for Poisson's ratio, a mean Young's modulus E of about 130 GPa can be deduced.
The electrical characterization was carried out by measuring the impedance/phase characteristics of different resonant structures.

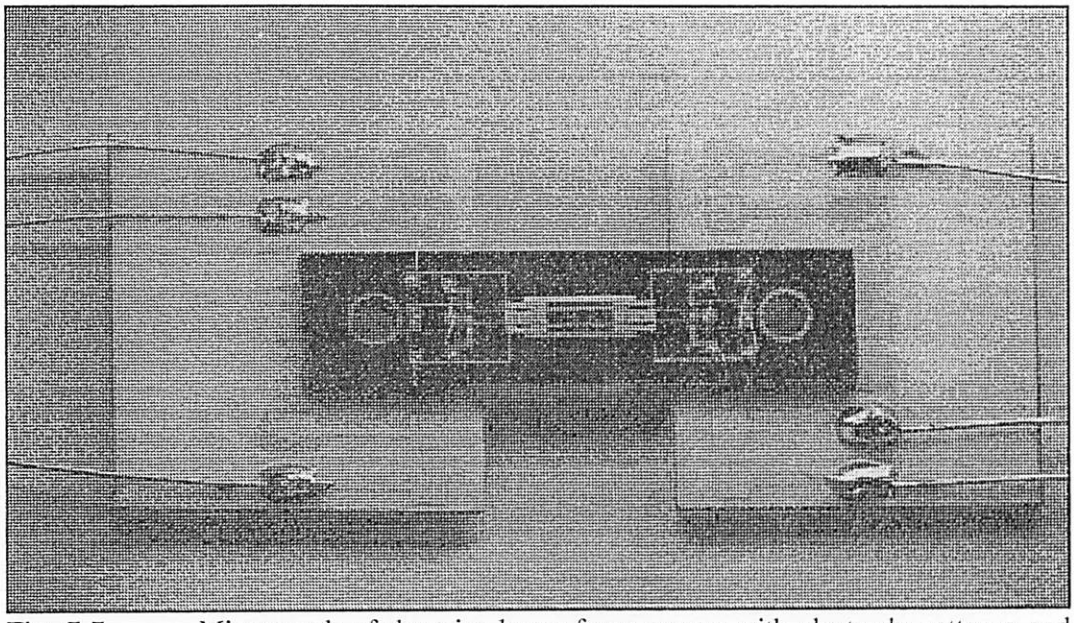

**Fig. 7.7** Micrograph of the tripe-beam force sensor with electrode patterns and bonding pads.

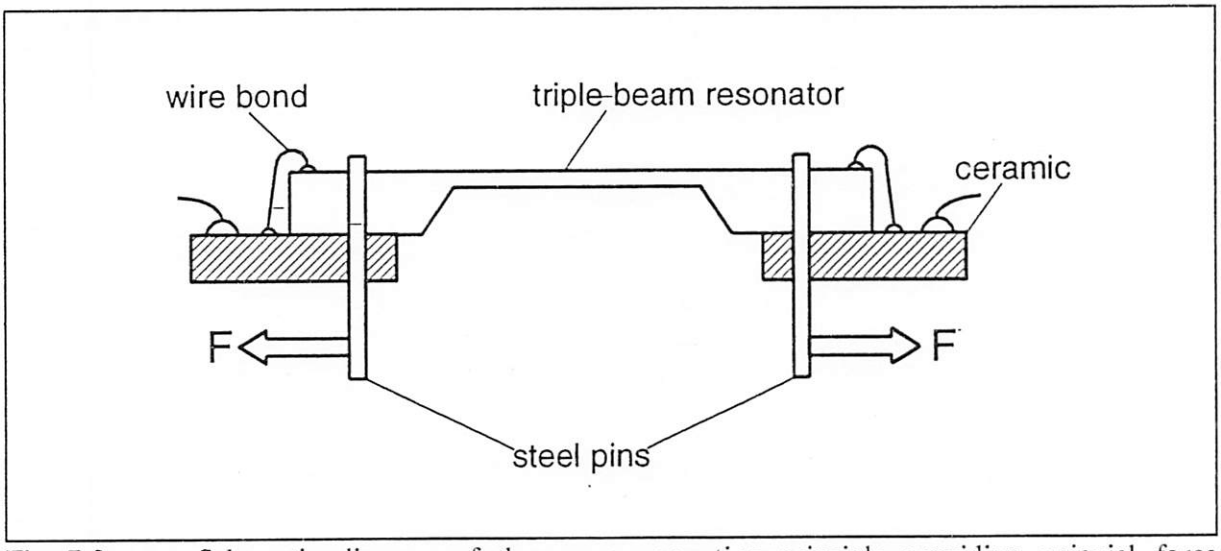


**Fig. 7.8** Schematic diagram of the sensor mounting principle providing uniaxial force measurements free of hysteresis.

The effective electromechanical coupling factors $k_{eff}^2 = (f_a^2-f_r^2)/f_a^2$ **[7.17]** were determined by measuring the fundamental resonance frequency $f_r$ and antiresonance frequency $f_a$ of the piezoelectric one-port resonators. Due to the dependence of $k_{eff}$ on resonator geometry, silicon/ZnO thickness ratio, and electrode configuration, measurements were correlated with piezoelectric FE-modelling results **[7.18]**. The measured $k_{eff}$ values for the triple-beam resonators were about 6-9% for an electrode deposited on 20% of the beam lengths at each side.

A laser vibrometer (POLYTEC OFV1102) was used to measure the mode spectrum of the resonators. Due to the optical readout, all electrodes could be used for excitation, resulting in a high mode selectivity for symmetrical modes. Enhancement of the mode-selective excitation in a real test environment might be achieved by employing a multiple electrode configuration **[7.19]**. Optically measured flexure mode spectra (M1, M2, M3) of a force

sensor with (a) coupled and (b) decoupled triple-beam resonators are shown in **Fig. 7.9**. The clamping of the coupled resonator is defined by the angle of the slow-etching (111) crystal planes of the silicon bulk. In this case there is no decoupling zone and therefore the modal behaviour exhibits a superposition of the three flexure modes (**Fig. 7.9(a)**).

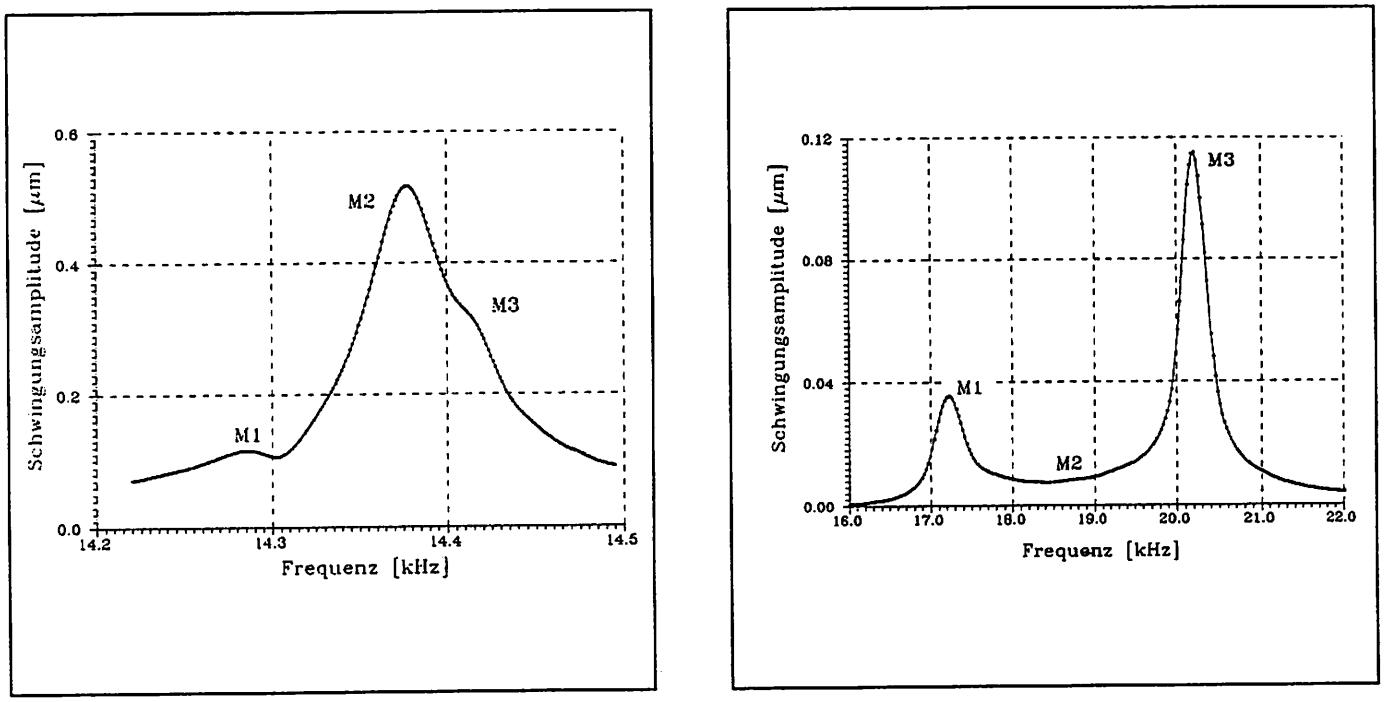


**Fig. 7.9** Optically measured flexure mode spectra (M1, M2, M3) of a force sensor with a mechanically (a) coupled and (b) decoupled triple-beam resonator.

The mechanically decoupled resonator with a decoupling zone length of 200 $\mu$m shows an increased mode splitting of 3 kHz (**Fig. 7.9(b)**). This value corresponds to an approximately 30 times higher mode splitting compared to the coupled resonator. The numerically calculated and measured resonance frequencies of the three flexure modes are summarized in **Table 7.3**, in which the resonance frequencies were normalized to the mode M1 ($c_i = f_i/f_1$). An assumed decoupling length of 50 $\mu$m (see **Fig. 7.4**) results numerically in a mode splitting within 1%., corresponding to the triple-beam resonator with bulk clamping, whereas a decoupling length of 200 $\mu$m leads to a frequency shift of 7% for mode M2 and 13% for mode M3, respectively. The numerical calculations are in satisfactory aggreement with the experimental results. Due to the optical readout at the centre beam, the decoupled resonator reveals a vanishing contribution of the vibration mode M2, which could be optically detected at the outer beams. The mechanical quality factors Q of the vibration modes increase from M1 to M3 by a factor of two. The maximum value of Q was measured to about 400 for mode M3 at ambient pressure conditions. The measured force/frequency characteristic of a triple-beam force sensor is shown in **Fig. 7.10**. The high residual stress of the ZnO thin film means that a V-shaped force/frequency characteristic is obtained. The measured force sensitivity is about 8.6 kHz/N for the right branch.
For sensor applications the residual stress has to be decreased in order to obtain a single-valued force-frequency dependence.

**Table 7.3** Comparison of calculated and measured splitting of resonance frequencies for the three flexure modes of a triple-beam resonator.

| | FE modelling | | Experimental data | |
|---|---|---|---|---|
| Decoupling length | 50 $\mu$m | 200 $\mu$m | bulk clamping | 200 $\mu$m |
| $c_1$ | 1.0 | 1.0 | 1.0 | 1.0 |
| $c_2$-1 | 0.3 % | 7.5 % | 0.5 % | 7.0 % |
| $c_3$-1 | 0.6 % | 14.1 % | 0.7 % | 13.0 % |

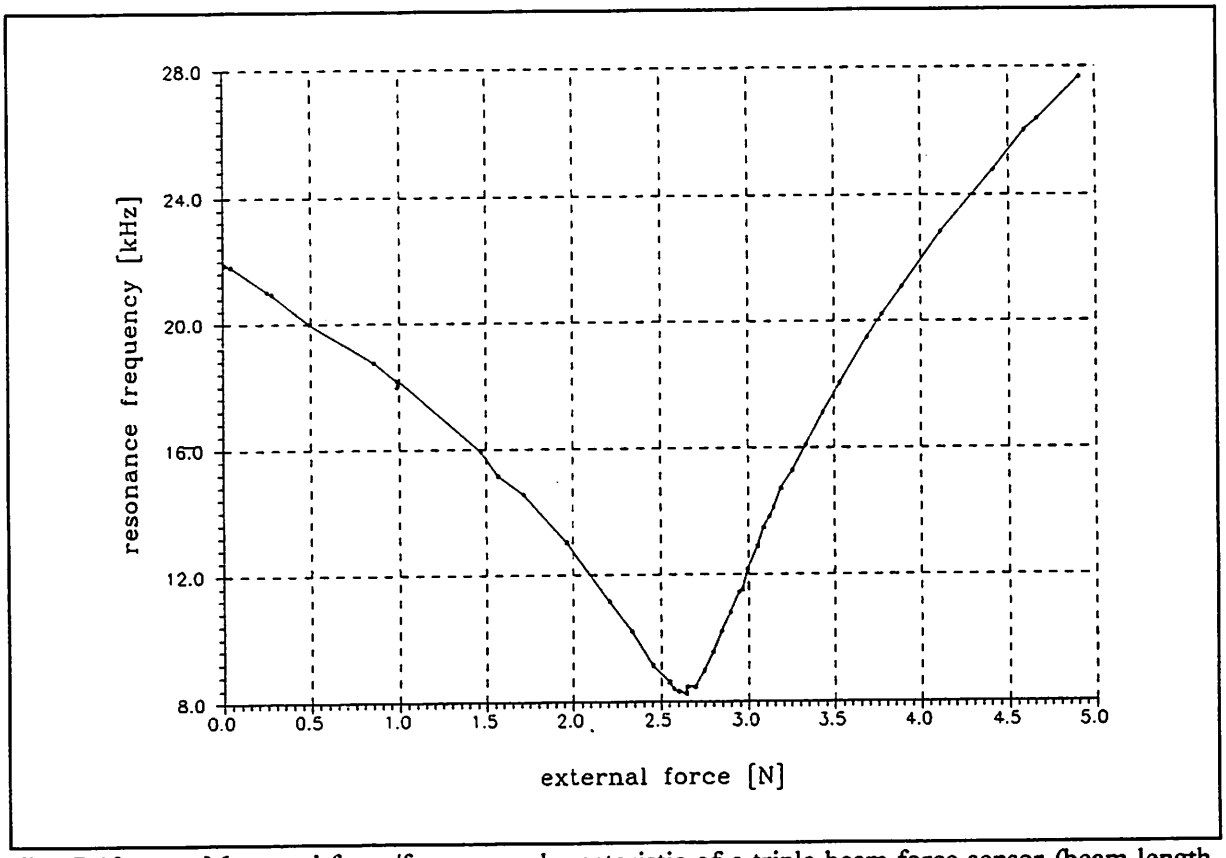


**Fig. 7.10** Measured force/frequency characteristic of a triple-beam force sensor (beam length, 3mm; beam thickness, 25 $\mu$m).

## 7.8 Conclusions

A triple-beam resonant force sensor with piezoelectric excitation was fabricated. Experimental characterization by means of optical and electrical measurement techniques was performed. The presented resonator configuration is capable of providing a sufficient mechanical isolation from the support by means of a flexibel decoupling region and at the same time reveals a better mode selectivity. In combination with vacuum encapsulation, in particular, the triple-beam resonator provides intrinsic advantages in comparison to single-beam resonators. The benefits of the presented resonator design seem to be promising for future resonant sensor applications.

## References Chapter 7*


[7.1] H.A.C. Tilmans, M. Elwenspoek and J.H.J. Fluitman, Micro resonant force gauges, *Sensors and Actuators A, 30* (1992), 35-53.

[7.2] G. Stemme, Resonant silicon sensors, *J. Micromech. Microeng., 1* (1991) 113-125.

[7.3] K. Ikeda, H. Kuwayama, T. Kobayashi, T. Watanabe, T. Nishikawa, T. Yoshida and K. Harada, Silicon pressure sensor integrates resonant strain gauge on diaphragm, *Sensors and Actuators, A21-A23* (1990) 146-150.

[7.4] J.C. Greenwood and D.W. Satchell, Miniature silicon resonant pressure sensor, *IEE Proceedings, Vol. 135, No. 5* (1988) 369-372.

[7.5] E.P. Eernisse, R.W. Ward and R.B. Wiggins, Survey of quartz bulk resonator sensor technologies, *IEEE Transactions on Ultrasonics, Ferroelectrics, and Frequency Control, Vol. 35, No. 3* (1988) 323-330.

[7.6] R.G. Kirman, A vibrating quartz force sensor, *Transducers TEMPCON Conference Papers, London, June 14-16, 1983, pp.98-121.*

[7.7] D.W. Satchell and J.C. Greenwood, A thermally-excited silicon accelerometer, *Sensors and Actuators, 17* (1989) 241-245.

[7.8] H.A.C. Tilmans, *Micro-mechanical sensors using encapsulated built-in resonant strain gauges*, Thesis, University of Twente, Enschede, The Netherlands, 1992.

[7.9] Swanson Analysis Systems, Inc., Houston, PA, USA.

[7.10] W.C. Albert, A low cost force sensing crystal resonator applied to weighing, *Proc. 42nd Annual Frequency Control Symposium, 1988, pp. 78-84.*

[7.11] M.V. Andres, K.W.H. Foulds and M.J. Tudor, Sensitivity and mode spectrum of a frequency-output silicon pressure sensor, *Sensors and Actuators, 5* (1988) 417-426.

[7.12] T. Aeugle, H. Bialas, K. Heneka and W. Pleyer, Large area piezoelectric ZnO film transducers produced by R.F. diode sputtering, *Thin Solid Films, 201* (1991) 293-304.

[7.13] F.R. Blom, D.J. Yntema, F.C.M. van de Pol, M. Elwenspoek, J.H.J. Fluitman and Th.J.A. Popma, Thin-film ZnO as micromechanical actuator at low frequencies, *Sensors and Actuators, A21-A23* (1990) 226-228.

[7.14] C.J. van Mullem, F.R. Blom, J.H.J Fluitman and M. Elwenspoek, Piezoelectrically driven silicon beam force sensor, *Sensors and Actuators A, 25-27* (1991) 379-383.

[7.15] M.J. Vellekoop, C.C.G. Visser, P.M. Sarro and A. Venema, Compatibility of zinc oxide with silicon IC processing, *Sensors and Actuators, A21-A23* (1990) 1027-1030.

[7.16] J.T. Kung, A.N. Karanicolas and H.-S. Lee, A compact, inexpensive apparatus for one-side etching in KOH and HF, *Sensors and Actuators A, 29* (1991) 209-215.

[7.17] R. Lerch, Simulation of piezoelectric devices by two- and three-dimensional finite elements, *IEEE Transactions on Ultrasonics, Ferroelectrics, and Frequency Control, Vol. 37, No. 2* (1990) 233-247.

[7.18] Th. Fabula, Dynamische Berechnungen in der Mikromechanik - Simulation /Messung, *10. ANSYS User's Meeting, Arolsen, Germany, October 28-30, 1992.*

[7.19] K. Funk, T. Fabula, G. Flik and F. Lärmer, Piezoelectrical driven resonant force sensor: fabrication and crosstalk, *to be published.*

[7.20] Th. Fabula, H.-J. Wagner, B. Schmidt and S. Büttgenbach, Triple-beam resonant silicon sensor based on piezoelectric thin films, *Sensors and Actuators A, 41-42* (1994) 375-380.

* Oral presentation is based on further references:

[7.21] A. Prak, *Silicon resonant sensors: operation and response*, Master's Thesis, University of Twente, Enschede, The Netherlands, 1993.

[7.22] Final report of the project: Einsatz der Mikromechanik zur Herstellung frequenzanaloger Sensoren, supported by the Bundesministerium für Forschung und Technologie (BMFT) under contract number 13 AS 0114 (1.7.89 - 31.12.92) in: Reihe Innovationen in der Mikrosystemtechnik, Vol.7, Ed.: VDI/VDE-Technologiezentrum Informationstechnik GmbH, Teltow, Germany, 1994.

[7.23] F.R. Blom, *Resonant silicon beam force sensor*, Thesis, University of Twente, Enschede, The Netherlands (1989).

[7.24] F.R. Blom, F.C.M. van de Pol, G. Bauhuis and Th.J.A. Popma, R.F. Planar magnetron sputtered ZnO films II: Electrical Properties, *Thin Solid Films, 204* (1991) 365-376.

[7.25] J.L. Deschanvres, P. Rey, G. Delabouglise, M. Labeau, J.C. Joubert and J.C. Peuzin, Characterisation of piezoelectric properties of zinc oxide thin films deposited on silicon for sensors application, *Sensors and Actuators A, 33* (1992) 43-45.

[7.26] X. Ding, W.H. Ko, Y. Niu and W. He, A study on silicon-diaphragm buckling, *Techn. Digest IEEE Solid-State Sensor and Actuator Workshop, Hilton Head Island, SC, June 4-7, 1990, pp. 128-131.*

[7.27] U. Erdem, Force and weight measurements, *J. Phys. E: Sci. Instrum., Vol. 15* (1982) 857-872.

[7.28] F.S. Hickernell, ZnO processing for bulk- and surface-wave-devices, *Proc. Ultrasonics Symposium, 1980, pp. 785-794.*

[7.29] F.S. Hickernell, Post-deposition annealing of zinc oxide films, *Proc. Ultrasonics Symposium, Chicago, IL, October 14-16, 1981, pp. 489-492.*

[7.30] F.S. Hickernell, Zinc oxide films for acoustoelectric device applications, *IEEE Transactions on Sonics and Ultrasonics. Vol. SU-32, No. 5* (1985) 621-629.

[7.31] U. Lindberg, J. Söderkvist, T. Lammerink and M. Elwenspoek, Quasi-buckling of micromachined beams, *J. Micromech. Microeng., 3* (1993) 183-186.

[7.32] C.J. van Mullem, *Micromachined silicon integrated resonant sensors*, Master's Thesis, University of Twente, Enschede, The Netherlands, 1993.

[7.33] F.C.M. van de Pol, Thin-film ZnO - properties and applications, *Ceramic Bulletin, Vol. 69, No. 12* (1990) 1959-1965.

[7.34] F.C.M. van de Pol, F.R. Blom and Th.J.A. Popma, R.F. planar magnetron sputtered ZnO Films I: Structural properties, *Thin Solid Films, 204* (1991) 349-364.

[7.35] A.D. Sathe and E.S. Kim, Techniques to control residual stress in ZnO thin films, *Proc. 7th Int. Conf. Solid-State Sensors and Actuators (Transducers '93), Yokohama, Japan, June 7-10, 1993, pp. 158-161.*

[7.36] S.M. Sze, *Physics of semiconductor devices*, 2nd ed., John Wiley & Sons, New York, 1981.

[7.37] J.A. Thornton, High rate thick film growth, *Ann. Rev. Mater. Sci., Vol. 7* (1977) 239.

[7.38] H.A.C. Tilmans, D.J. Ijntema and J.H.J. Fluitman, Single element excitation and detection of (micro-)mechanical resonators, *Proc. 6th Int. Conf. Solid-State Sensors and Actuators (Transducers '91), San Francisco, CA, U.S.A., June 23-27, 1991, pp. 529-532.*

[7.39] R.H. Williams, Interfaces in semiconductor structures and devices, *Phys. Blätter, 45* (1989) 219-223.